Plasma Wind Tunnel Demisability Testing of Spacecraft Equipment

James Beck [a], Antonio Caiazzo [b]*, Ali Gülhan [c], Luisa Innocenti [d] Thorn Schleutker [e], Tiago Soares [f]

[a] *Belstead Research (BRL), United Kingdom, james.beck@belstead.com*
[b] *European Space Agency (ESA -ESTEC), The Netherlands, antonio.caiazzo@esa.int*
[c] *German Aerospace Centre(DLR), Germany, ali.guelhan@dlr.de*
[d] *European Space Agency (ESA -HQ), France, luisa.innocenti@esa.int*
[e] *German Aerospace Centre(DLR), Germany, thorn.schleutker@dlr.de*
[f] *European Space Agency (ESA -ESTEC), The Netherlands, tiago.soares@esa.int*
* Corresponding Author

Abstract

In previous activities on-ground testing in Plasma Wind Tunnels (PWT) that reproduce the plasma environment during re-entry have been used to characterize the behaviour of materials and simplified satellite structure samples at representative conditions. However, major uncertainties in the demise process are the fragmentation events occurring at both system and equipment level during the re-entry which can drive the casualty risk estimate. Parts that are predicted to produce a single ground-reaching fragment in today's state of the art simulations may actually generate several objects, having a severe impact in the overall casualty risk estimation.

With regard to these knowledge gaps, ESA Clean Space initiative has launched a new activity with Belstead Research Limited and the German Aerospace Centre (DLR) under the name of *Spacecraft Equipment Characterisation in Re-Entry Tests* (SECRET). The objective of this activity is to characterize the break-up processes of critical spacecraft elements through destructive on-ground re-entry tests to be performed in a Plasma Wind Tunnel. This work foresees significant improvement in the understanding of critical spacecraft elements and the on-ground re-entry experiments through testing and subsequent reconstruction in re-entry simulation tools. Development of representative models to capture missing, or poorly modelled, processes observed in the tests is planned.

In the frame of this activity, complex pieces of equipment are tested in the DLR L2K Plasma Wind Tunnel facility. These tests are essential to understand the break-up phenomena of that equipment, to improve the risk estimation and to implement effective D4D measures. The test results analysis provides a better understanding for the derivation of recommendations for Design for Demise. Further investigations are needed, taking also into account an improvement of the set-up of the experiments. Therefore, the post-test data analysis will provide a better understanding of the destructive processes of the selected hardware, for the benefits of prediction models and design for demise recommendations. The results will help to gain a deeper understanding of D4D for the benefit of early-phase space mission studies within space industries.

Keywords: Space Debris Mitigation, ESA CleanSat, Design for Demise, Plasma Wind Tunnel test

1. Introduction

In the last few years, it become clear the need of guidelines for an assessment of the survival probability for re-entering objects. Such guidelines will help during the design process of a satellite in order to decide, whether a controlled re-entry had to be foreseen at the end of the lifetime, or an uncontrolled re-entry would be acceptable. In this direction, several activities and simulations have highlighted a number of critical spacecraft elements that tend to at least partially survive re-entry conditions and pose risks on the ground. In order to improve our prediction models and the understanding of the demise behaviour of critical components there is the need for on-ground tests.

According to simulations, parts may result in a single fragment reaching the ground. But the reality might be different: pieces which in simulation should result in a single fragment, may actually generate several smaller pieces of debris. Basically put, the more pieces you have, the highest the overall casualty risk estimation will be. To help fill knowledge gaps in the re-entry analysis and Design for Demise fields, the activity 'Characterisation of behaviour of critical elements in re-entry conditions' aims to characterise the break-up process of critical spacecraft elements through destructive on-ground re-entry tests to be performed in a Plasma Wind Tunnel (PWT). This work foresees the identification of critical spacecraft elements and the on-ground re-entry experiments through test reconstruction in re-entry simulation tools.

2. Test Facility

A spacecraft re-entering Earth's atmosphere experiences severe aerothermal and mechanical loads. The thermal loads mainly consists of two types; convective heat flux and radiative heat flux. In order to study the demisability process of the commonly used materials and critical components subjected to these loads, several tests could be done which mimic the re-entry environment. There are two main types of test facilities; Static heat facilities and Dynamic test facilities. In this activity, the tests have been done in a plasma wind tunnel facility (dynamic test facility) at DLR, Cologne. Plasma wind tunnel facilities can provide a high-enthalpy gas flow environment in various conditions that characterise re-entry trajectories from Low Earth Orbit (LEO). The varying conditions consists of the working gas' composition and mass flow rate, heat flux, ambient pressure etc. The boundary layer that the specimen is subjected to, is thermodynamically akin to atmospheric re-entry, although the flow velocities are comparatively low, typically from transonic to low hypersonic Mach regimes. This is compensated by a plasma generator, which increases the flow enthalpy to provide the equivalent total pressure, local mass-specific enthalpy and the velocity gradient at the boundary layer edge, thus achieving boundary layer similarity. In addition, the latter condition is achieved by scaling the effective nose radius of the specimen, thus enabling the scaling and correlation of the stagnation point heating conditions to ensure the local thermochemical similarity given the calibrated PWT test scenario and the flight reference.

Figure 1: Plasma Wind Tunnel L2K Facility (view from inside)

The L2K facility is one of the wind tunnels in the Hypersonic Technology Department of DLR Cologne, used for the tests in the frame of this activity. Along with the higher pressure L3K tunnel, it is part of the LBK facility. Significant advantages of the LBK tunnels are that they are supersonic and run at Mach numbers of between 4 and 8. Whilst well below the flight Mach number (~Mach 25), it is better than many arc-heated facilities, which run in either the subsonic or transonic range, allowing something of the shock structure to be understood.

The heat flux is highly dependent upon the geometry of the test object, and can be difficult to obtain on objects where there are multiple length scales. Tighter curvature results in smaller shock standoff distances and thus increased velocity gradients at the surface and so higher local heat transfer. As such, it is difficult to calibrate a heat flux based on a complex geometry, and ideally each sample would have its heat flux calibrated using a calibration object of the same shape as the test sample. As this is not economic in practice, the calibration is performed on a flat faced cylinder, and the cold wall heat flux to the surface of objects is inferred from standard correlations for known shapes and representative length scales. In order to ensure that the key phenomenology are captured, whilst maintaining the possibility of obtaining quantitative data from steady state energy balances, an innovative approach to the test conditions is proposed. In this concept, a set of conditions are calibrated at varying heat flux at the same sample location such that they can be stepped through during the test.
This allows, for example, a test to:

- Start at 300kW/m2 and obtain a steady state
- Move to 400kW/m2 and observe the demise of some parts and reach a second steady state on a more resistant part
- Finally move to 500kW/m2 and observe the demise of the more resistant part.

This also allows for adjustment to higher fluxes if the demisability of a part is underestimated, increasing the probability of observing the desired phenomena. This can happen for two major reasons. Firstly, the emissivity of the test object is higher than the predicted value. Many quoted emissivity values are substantially below those observed in demise testing. Very conservative values have been used in the conditions selection within this activity, and found to be reasonably accurate. Secondly, the wind tunnel enthalpy is lower than expected. The equilibrium conditions obtained are also highly dependent upon the facility enthalpy as this determines the reduction in the heat flux to the surface of the test object as its temperature increases. Low estimated values of enthalpy can result in erroneous predictions of no demise when the sample clearly reaches a demise condition.

3. Equipment and tests

A number of spacecraft demise studies, both experimental and through simulations, have been performed recently. These have confirmed much that was expected, but have also enhanced the understanding of the demise processes as well as demonstrating that there are still significant unknowns which are not well represented in demise models. These issues highlight the need for spacecraft equipment to be properly demise qualified, inclusive of testing, as this provides a starting point to ensure that the understanding of demise behaviour is sufficient to draw conclusions on the criticality of the item. In order to assist the selection of items for testing in this campaign, studies of the equipment were critically assessed, and compared with the findings from the previous test campaigns. This was done from an equipment viewpoint in order to understand the key phenomena to be tested for each type of equipment, in order to improve the understanding of demisability.
From these studies, a set of items of interest were prioritized. These (with reasons) are

- Reaction Wheels (to test alternate material flywheels).
- Solar Array Drive Mechanisms (in support of simulation data, assessment of critical items).
- Batteries (verification of fragmentation to cells).
- Magnetorquers (verification of layer-by-layer demise)
- Electronics Boxes (fragmentation process, behaviour of GFRP cards)

Five test categories have been selected. These are magnetorquers (MTQ), RW90 reaction wheel, electronics boxes, battery cells and modules and reaction wheel ball bearing units.

3. 1 Magnetorquer

The MTQ is shown in Figure 2 in the set-up for the plasma wind tunnel test. This is made up of a cobalt/iron alloy core, surrounded by copper wire layers, separated by insulating tape. There is then a layer of potting material with a CFRP outer shell.

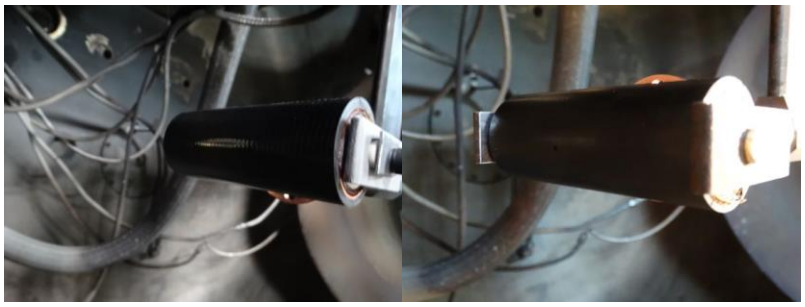

Figure 2: Test 1 MTQ (left) Test 2 MTQ without housing (right)

The CFRP housing is of interest as previous test have suggested that this might act as an effective heatshield, protecting the internal parts as has been seen in overwrapped tanks found on ground. This is particularly the case as there might be hoop stresses in the carbon fibres due to the curvature of the wrapping which would make them more likely to stay in place. Therefore the test was performed with a 90mm section of the magnetorquer normal to the flow. A second test without the CFRP housing has also been performed, as it would be expected that a demisable magnetorquer design would not use a CFRP housing.
The primary interest in the magnetorquer testing is the layer- by layer demise, therefore, the desired setup is with the layup in the flow direction and the axis of the magnetorquer normal to the flow. This results in the curved surface of the magnetorquer in the flow such that the flux on the side will be non-uniform.

The two magnetorquer tests were successfully performed, and resulted in the expected phenomenology. In the first test, the following observations were made:

- The CFRP burnt through at the 542kW/m2 condition significantly more quickly than expected.
- The copper coils do not behave as solid copper due to the insulation between them causing a very low net conductivity. The failure is thus layer-by-layer. The copper also forms a conduction path to the sample holder resulting in significant heat losses.
- Equilibrium is reached with the copper removed at the 542kW/m2 condition, and a second equilibrium is reached at the 642kW/m2 condition.
- The core is observed to melt at the 749kW/m2 condition.

Figure 3: Test MTQ with housing events sequence

The behaviour in the second test without the CFRP housing was largely similar, with the potting being removed within 20s. In addition, the two-colour pyrometer data suggests an emissivity of 0.75-0.8 for the copper coils and 0.8-0.85 for the cobalt/iron core. These figures are consistent with both sets of equilibrium data. A layer-by-layer approach is confirmed to be appropriate for demise modelling.

3. 2 Reaction Wheel

The RW90 reaction wheel and its copper-beryllium (CuBe) flywheel are shown in Figure 4. The expected demise behaviour of the reaction wheel is a removal of the aluminium housing and a later demise of the flywheel. Therefore, two tests were performed. The first examines the wheel assembly, with the sample mounted by the flywheel to observed the housing failure. The second is performed at higher flux on the flywheel alone in order to observe the CuBe material failure.

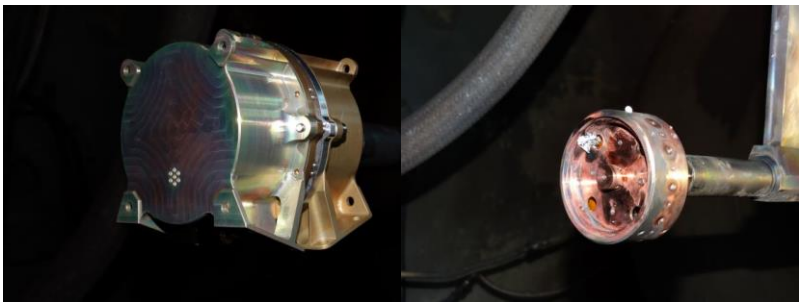

Figure 4: Test 3 RW90 (left) Test 4 Flywheel (right)

From previous tests, it is known that aluminium will melt at the lowest heat flux level of 100kW/m2, and that this condition is suitable for demise of the housing, but was expected to leave the copper flywheel intact, and available for a further test. The copper flywheel is slightly smaller than the calibration sample, and therefore, the fluxes are predicted to be slightly higher as shown in Table below. As there is some uncertainty over the melt temperature emissivity of the CuBe, a set of higher flux conditions are given, even though melt is expected at the 300kW/m2 nominal flux condition.

The two planned tests were performed successfully, with the melt of the CuBe being observed at the 300kW/m2 heat flux as anticipated. The following observations were made in the first test:

- The aluminium housing fails by tearing of the oxide layer (Figure 5) once there is sufficient molten material inside to allow it to move.
- The internal aluminium cage around the motor continues to fail, and eventually the rear housing also fails. The remaining parts are the motor, which has steel parts within an aluminium housing, and the flywheel (Figure 5).

Figure 5: Test RW90 events sequence (from left to right)

The survival of the motor housing was not expected, and suggests that the steel internal parts were able to act as a heat sink. This was partly shielded by a part of the front housing remaining attached to a thermocouple situated on the front face. As this oxide film on the thermocouple was in the line of sight of the pyrometer, the temperature reading was able to validate the two-colour pyrometer estimate of the emissivity. The temperature agreement was very good and the oxide emissivity is estimated at 0.5.

The flywheel was then remounted and tested, starting at 200kW/m2, reaching equilibrium, and then moving to 300kW/m2. The following observations were made:

- The flywheel is close to isothermal given the high conductivity of CuBe, but higher fluxes can be observed at the centre and the rim due to the geometry of the flywheel (Figure 6). Equilibrium is reached at 200kW/m2, consistent with the measured emissivity of 0.75.
- At 300kW/m2, the flywheel is observed to melt first at the rim, and then in the centre (Figure 6).

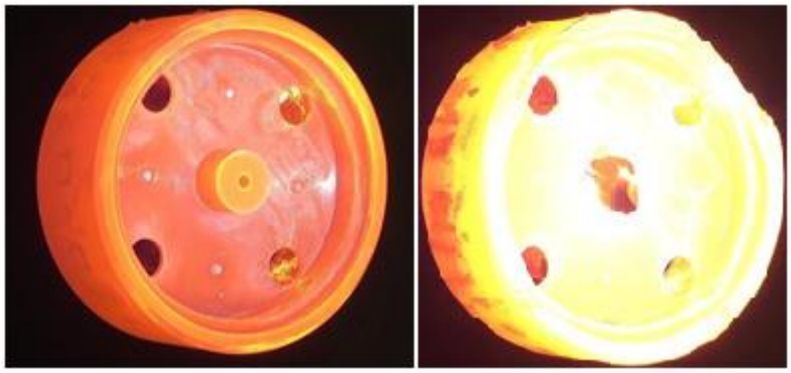

Figure 6: Test Flywheel events sequence (from left to right)

The results suggest that a relatively simple component-by- component failure model is applicable for objects with aluminium housings and less demisable interior components, and further demonstrates that the use of a CuBe flywheel provides a significant improvement in demisability over a stainless steel material, whilst maintaining a similar density.

3. 3 Electronic Box

The electronics box is shown in Figure 7. The box itself was too large for the wind tunnel, so a section was cut, which includes a backplane connected to four electronics cards. The purpose of this test was to establish the fragmentation behaviour, specifically whether the cards are easily removed.

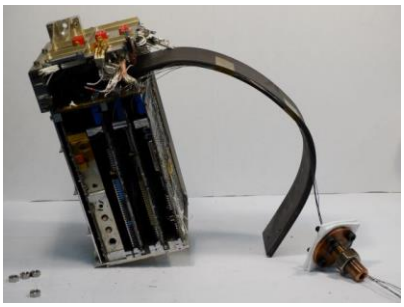

Figure 7:Test 5 Electronics Box set-up

The results of the first test suggested subsequent tests on the cards themselves. Two cards were selected, shown in Figure 8. The card on the left has power conditioning circuitry mounted on a two layer printed circuit board. The components, including coils, resistors and capacitors, were considered representative of power supplies and similar hardware. The card on the right is representative of a digital logic board with integrated circuits, housed in ceramic packages, mounted on a multi-layer PCB.

Figure 8: Test 6 and 7 Electronics Cards

As the electronics box has a similar aluminium housing the 100kW/m2 condition is appropriate. For the individual cards, the behavior of the GFRP material is not well known, and so the fluxes are stepped up from 100kW/m2 to the point where demise is observed.

All three tests were performed successfully. The following observations were made on the test on the electronics box section:

- The aluminium housing fails due to tearing of the oxide layer consistently with previous observations.
- There is significant charring of the exposed electronics, but no clear demise (Figure 10).
- Detachment of the front card is observed, but sufficient housing remains that the cards stay in place.
- The four electronics cards lose connection to the backplane and a complete separation is observed.

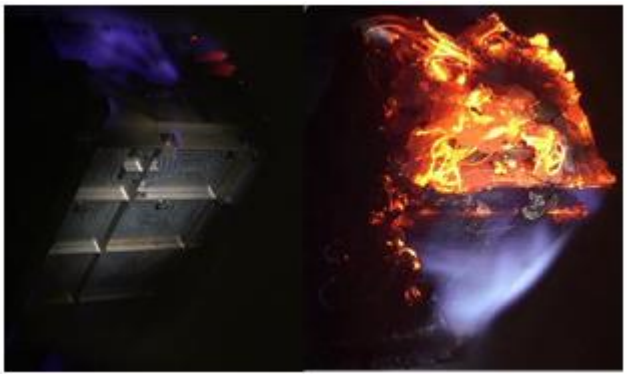

Figure 9: Electronics Box at Start and After Housing Removal (from left to right)

As the separation of the cards from the backplane is complete, the modelling of electronics boxes as a housing with internal cards, such that the cards are released separately on the failure of the housing is supported by this test. Given this outcome, the tests on individual cards become more important as this is key to ensuring the demise of electronics components.

The observations from the two tests on the electronics cards were remarkably similar, which has suggested that a single model could be used in simplified codes to represent a generic GFRP electronics card. The observations are given below, with the Figures shown from the first card test:

- At 100kW/m2, there is charring of the GFRP card, and the aluminium frame is removed (Figure 10).

- Some of the steel parts are observed to inflate, and some parts are removed from the card (Figure 10).
- An equilibrium is reached, and the flux is increased to 200kW/m2. At this condition, the card bends and the glass material can be seen to reach a lower viscosity, but there is no major flow (Figure 10).
- A second equilibrium is reached, and the flux is increased to 300kW/m2.

The failure of the cards is achieved at significantly higher temperatures than are used in current models. The first equilibrium surface temperature (100kW/m2) is at approximately 8300C, and the second (200kW/m2) is at approximately 10600C. The removal of large amounts of material is observed at 12000C, which is recommended as a proxy melt temperature for simplified models. This is substantially higher than has been used previously. The emissivity measurements suggest a value of 0.9 should be used.

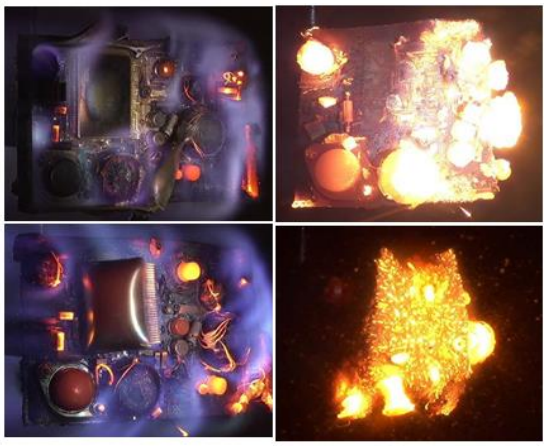

Figure 10: Test 6 (left) and 7 (right) Electronics Cards events sequence

3. 4 Ball Bearing Units

The ball bearing units tested are shown in Figure 11. The right hand image is of a mock-up of a similar, but longer unit. Importantly, the leading edge of the mock-up is not closed such that the geometry of the two stainless steel items is different.

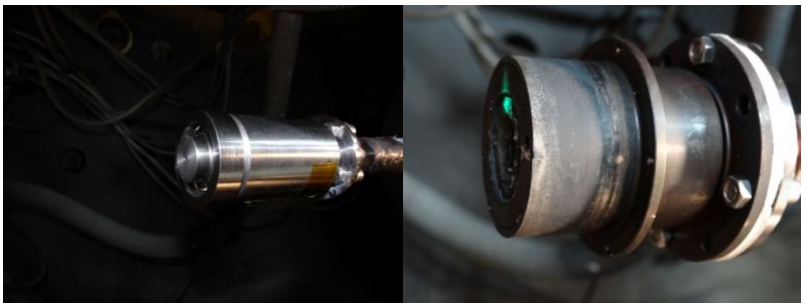

Figure 11: Test 8 and 9 Ball Bearing Units

The conditions on the ball bearing units have been selected based on the highest achievable heat flux (1.5MW/m2) in the L2K facility. Predictions suggested that melt would occur at 1.3MW/m2, so the tests were started at this condition, and then adjusted to 1.5MW/m2 within the first minute of the test. For both the mock-up and the ReDSHIFT unit, melt was observed at the lower flux condition.

The difference in the leading edge geometry of the two objects (see Figure 12) results in significantly different demise behavior at the start of the test. The key observations are as follows:

- Immediate melt is observed on the mock-up where the first melt is observed at 1 minute on the ReDSHIFT unit.
- First visible recession of the leading edge of the mock- up is at 23s (Figure 13).
  - An oxide layer is continually being formed and removed in each case. The oxide is less well formed on the ReDSHIFT unit. The objects become geometrically similar.
- The recession rates become similar once the leading edge geometry has receded and both behave as a receding tube of stainless steel.
- No equilibrium is reached, both units continue to demise.

Figure 12: Mock-up at 23s (left) and ReDSHIFT unit at 45s (right)

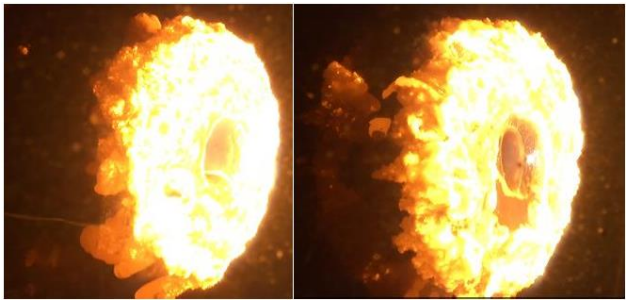

Figure 13: Mock-up (left) at 187s, ReDSHIFT unit (right) at 170s

The recession rates shows the earlier recession of the mock-up unit, and the similar recession rates obtained later in the test. Therefore, the shape of the object is highlighted as having a significant impact on the heat flux received. The emissivity data is also interesting in these tests as this suggests that the emissivity is approximately 0.8 prior to melt for the ReDSHIFT unit, but that this value drops to approximately 0.6 whilst the object is melting. A similar drop is also noted in other tests, suggesting that this is potentially of benefit for use in simplified demise models.

3. 5 Battery

Battery cells of three charge states (charged at 4.2V, discharged at ~1V, and passivated at ~0.5V) are tested together as shown in the left hand pane of Figure 15, and a single passivated cell is shown in the right hand pane. The single cell test was performed as a result of the initial three cell test being run at incorrect test conditions.

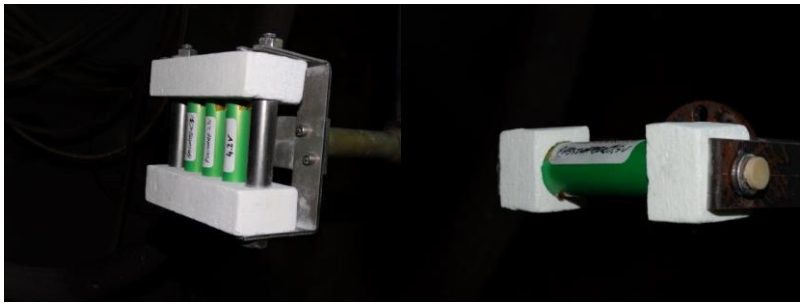

Figure 15: Test 10 and 12 Battery Cells

Two battery modules were also tested, similarly due to an error in the conditions of the first test. The modules contained 16 cells between two GFRP sheets as shown in Figure 16. Although the conditions are not well known for the first of these tests, the data has still been used.

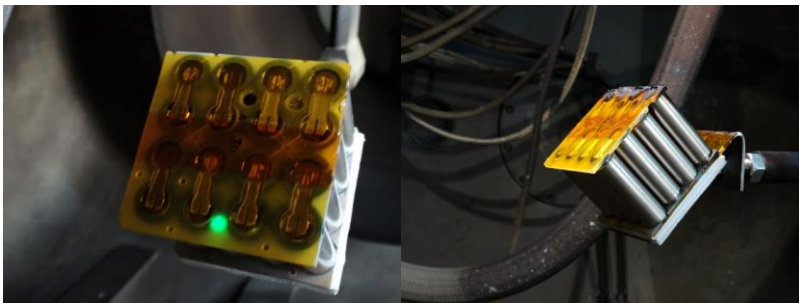

Figure 16: Battery Module

The purpose of the battery cell tests was twofold; firstly to confirm that the cells are demisable at the predicted conditions which are determined by the melt of the mild steel can, and secondly to understand the effect of the internal chemistry – thermal runaway – on the demise. Although the first test was run at a higher than intended heat flux with a flow core which is too small for the sample, the impact of the charge state was clear, as shown in Figure 17, where the charged cell demonstrates thermal runaway before the others. It is worth noting that the cells reach the same equilibrium at the first flux condition, demonstrating that the thermal runaway may affect the speed of demise, but is not determining of the demise itself.

Figure 17: Thermal runaway evident in charged cell

Melt of the steel can is observed at approximately 300kW/m2 nominal flux, equivalent to an average of 750kW/m2 on the curved surface. This shows that the conductivity through the cell is reasonably low due to the different layers of the cell, which are visible in Figure 18 as the melt temperature of the steel can is reached at a condition where the equilibrium temperature would not predict melt.

Figure 18: Melt of steel can revealing cell layers

These tests provide sufficient evidence to suggest that the behaviour of the cells is well approximated by use of a steel material for a cell, and confirm that the demise of the cells is highly likely if fragmentation to cells occurs.

The module tests are designed to determine whether this fragmentation is likely to occur. It is very interesting to note that the behaviour of the GFRP plates is very similar to that observed in the electronics cards, although the emissivity is significantly lower.

These tests were started at 100kW/m2, with the flux increased to 200kW/m2 at which point the surface melt of the GFRP was observed. At this point there was also a blow-out of the cells resulting in the connection to the lower plate of the first cell row being lost. This is shown in the left hand pane of Figure 19. The connection to the upper plate is maintained through the steel contacts between the cells.

Figure 19: Battery module demise

This resulted in the demise of the GFRP material being the driver for the fragmentation of the module, which occurs quite quickly once the GFRP reaches a temperature of approximately 12000C, consistently with the electronics card tests. At the heat flux required to reach this temperature (300kW/m2), the cells were also beginning to demise. Interestingly, the release of the connection of the cells to the bottom plate allowed the flow around the cells to change such that the local heat flux significantly increased. This suggests that the flow path is required in order to see the full effect of the local curvature on the heat flux, but that the size of the flow path can be reasonably small.

The demise of the GFRP is reasonably slow, such that a three layer model is recommended for batteries, with the demise of the outer housing, followed by the demise of the GFRP layer to allow fragmentation to cells, and finally the demise of the cells themselves. This provides a more conservative model than has been used in previous SAM assessments [2], and further work is required to determine whether this affects the demise criticality of large batteries

4. Conclusions and recommendations

A very large amount of useful demise data has been collected in a set of tests on critical equipment, which has employed an innovative stepped heat flux profile in a number of tests in order to obtain valuable equilibrium data. These results have validated the emissivity data obtained from pyrometers, and consolidated modelling of the wind tunnel flow enthalpy. This methodology is highly recommended for future demise tests.
Capturing of the correct flux levels for testing has been successfully achieved via mapping of the calibration flux levels to the test object geometry. This is non-trivial, and is critical to obtaining the desired test data.

A number of demise processes which have been inferred based on engineering judgement have been confirmed, which is useful for the application of models in simple demise tools:

- Layer-by-layer demise of magnetorquers
- Aluminium housing failures releasing less demisable parts
- Release of individual electronics cards from electronics boxes.
- High demisability of copper-beryllium relative to steel
- Fragmentation of batteries to cells is expected

As well as this, a number of observations were different from expectations and are worthy of further investigation:

- Low demisability of GFRP electronics cards
- Fragmentation of batteries to cells is driven by GFRP failure, which occurs later than expected
- Relatively early failure of the magnetorquer CFRP housing
- Low copper coils conductivity due to wiring insulation
- Survival of the aluminium motor shell
- The large shape effect in the ball bearing unit demise
- The emissivities measured are substantially higher than those used in many demise tools.

References

[1]J. Beck et al., “Plasma wind tunnel demisability testing of spacecraft equipment”, ESA Final Presentation, 2019.

[2]N. Leveque et al., “Multi-disciplinary assessment of design for demise techniques”, D4D-PS-ADSS-SY-10000128624, ESA Final Presentation, 2016.